JOURNAL OF MATERIALS SCIENCE 26 (1991) 6764–6776

Compression fracture of unidirectional carbon fibre-reinforced plastics

S. L. BAZHENOV*, V. V. KOZEY
Institute of Chemical Physics, Kosygin St. 4, 117977 Moscow, USSR

The effect of volume fraction and tensile strength of fibres, temperature and stress concentrators on the compression strength and fracture mode of unidirectional CFRP was studied. The cause of kinking is different for composites reinforced by low- (< 3 GPa) and high-strength fibres. If fibre strength is high, the kink is initiated by composite splitting followed by fibre bend fracture in the tip of the split. In the case of low-strength fibres, kinking is initiated by compressive fracture of the fibres. The effect of stress concentrators on the CFRP compressive strength is described by linear fracture mechanics. In the presence of defects, fracture is a result of the emergence of splits near a hole. As the critical stress of splitting growth initiation reduces in proportion to the square root of the defect size, the Griffith criterion describes the composite compressive fracture. At elevated temperature, failure is caused by fibre buckling. The fracture band in this case is oriented perpendicular to the fibre direction. Carbon fibre compressive strength may be measured by the loop method. Bending a strand of carbon fibres glued to the elastic beam gives a fibre-controlled upper limit of the composite compressive strength.

1. Introduction

There are several different models describing the failure of unidirectionally reinforced composites under compression load applied along the fibre direction. Historically, the first to appear was introduced by Dow and Gruntfest [1] and by Rabinovich [2], according to which, failure is a result of fibre buckling in a fashion analogous to the buckling of a column on an elastic foundation [1, 2]. Compressive strength, σ_c', in this model is described by the Rabinovich equation [2]

$$\sigma_c' = G_m/(1 - V_f) \quad (1)$$

where V_f and G_m are the fibre volume fraction and the matrix shear modulus.

Over the last three decades a variety of papers has been devoted to the study of this fracture mode. However, experimental investigations produced numerous results contradicting this model. (1) According to Equation 1 compressive strength should be equal to 3–5 GPa if conventional epoxy resin is used as a matrix. However, in reality, the strength of carbon fibre-reinforced plastics (CFRP) does not exceed 1.6–1.8 GPa [3–7]. (2) Composite compressive strength is proportional to the fibre volume content, V_f [4], while in accordance with Equation 1 it is expected to be non-linear. (3) Strength depends on the fibre types. It decreases with increase in fibre elasticity modulus [5–7]. (4) A direct proportionality between compressive and shear strengths of CFRP is observed [6].

The discrepancy between theory and experiment led to the conclusion that failure is caused not by the fibre buckling, but by some other reason. According to Weaver and Williams [8] and Parry and Wronski [9] the failure may be a result of the composite longitudinal splitting (delamination) and consequent buckling of the outer split layers. In glass fibre-reinforced plastics (GFRP) the proportionality between the compressive and shear strengths is the most characteristic feature of splitting [10]. Summarizing various literature data Petker [6] has pointed out the same proportionality for CFRP. This proportionality indicates the important role of splitting on CFRP compressive failure. On the contrary, the appearance of fractured samples does not confirm it. In CFRP splitting is observed only if the samples are tested without any guides preventing the specimen distortion and crushing of their butt-ends. The strength values (~ 0.5 GPa) are two- to four-fold lower than in up-to-date test methods. As a rule, the failure of CFRP is a result of the appearance of so-called kinks (shear bands) [3, 4, 11–13] at some angle ($\sim 45°$) to the fibre axis.

Another fundamental approach to the problem of compressive failure, according to which the composite strength is limited by the compressive strength of the fibres themselves, was proposed by Evins [11], DeFerran and Harris [12] and Sierakowski *et al.* [13]. A similar idea is that of a composite "shear" fracture mode. The kink appears at an angle of $\approx 45°$ to the load axis, i.e. close to the plane of the maximum shear

* *Present address*: Department of Macromolecular Science, Case Western Reserve University, Cleveland, OH 44106, USA.

0022–2461/91 $03.00 + .12

stresses. For this reason, failure of CFRP was considered as "shear" and the cause of fracture was supposed to be shear fracture of the fibres [11–13].

Thus, numerous and sometimes contradictory fracture models of CFRP, i.e. "fibre buckling", "splitting", "kinking", "fibre fracture" and controlled by fibre strength "shear" mode, have been proposed. The only reliable result which is beyond doubt is that CFRP failure is the result of kinking. An important question is whether kinking is a separate fracture mode or it is a consequence of some another cause. For example, Argon considered kinking as a result of fibre buckling [15], initiated by some fibre oriented at some small angle to other fibres by analogy with dislocation slippage in metals (bent fibre stimulates buckling of neighbour fibres). Kinking has also been supposed to be a consequence of fibre shear fracture [12, 13].

If the composite strength is close to the fibre strength multiplied by their fraction, V_f, it is evident that the fibre's fracture is the real cause of kinking. Owing to the small diameter of the fibres, measurement of their compressive strength is quite a complicated task. There are three different methods of compressive strength measurements. In the first, a single fibre or strand of fibres embedded in an epoxy block is compressed [16, 17]. The strengths of pitch- and rayon-based fibres ($E_f = 250$ GPa) and of high modulus Tornel-50 fibres ($E_f = 355$ GPa) are evaluated as ≈ 2.2 and 1.7 GPa, respectively [16]. These values are close to or slightly lower than the fibre tensile strength. Fibre compressive strength significantly decreases if the elasticity modulus exceeds 350 GPa [16]. The compressive strength of superhigh modulus graphite fibres ($E_f = 510$ GPa) is estimated to be 1–1.1 GPa [17] which is almost half their tensile strength.

Allen [18] proposed a recoil test based on the idea that the compressive stress at the moment of arrival of the shock wave to the end tabs after a tensioned fibre has been cut, is equal to the initial tensile stress. The recoil method was successfully used to measure compressive strength of aramid fibres. For high-strength AS4 fibres and high-modulus pitch-based P-55 fibres, this method gives 1.44 and 0.40 GPa, respectively. These values are approximately half those for the fibre compressive strength, σ'_f, estimated from the composite strength, σ'_c, in accordance with the mixture law $\sigma'_f \simeq \sigma'_c/V_f$ as 2.7 [9] and 0.86 GPa [19], respectively. The possible cause of errors is the fibre bend fracture near the end tabs [18].

Oshawa *et al.* [20] measured the lengths of pieces of fibre embedded in a matrix after compression, and using Kelly and Tyson's equation [21] estimated the strength of PAN-based T-300 and M-40 fibres to be 2.06 and 0.78 GPa. In accordance with the mixture law, the strengths of these fibres in the composite are 2.7–2.9 GPa [7, 19] and 1.5 GPa (see Fig. 3 below), respectively. According to Bazhenov *et al.* [22] due to a matrix support effect, the compressive strength of organic aramid fibres in a composite may be higher than that of isolated fibres, but the increase in strength is equal to $\sigma_m V_m/V_f$, where σ_m and V_m are matrix strength and volume content respectively. An estimation of this value shows that in the case of CFRP composite with a fibre content $\sim 60\%$, the effect may be neglected (whether the matrix support effect could be neglected in the case of compression of a single fibre embedded in a polymer matrix is not clear). Thus, the fibre strength values measured by different methods do not agree; the last two methods contradict the mixture law, and the problem of carbon fibre strength measurement has not been solved.

In several papers an equality of compressive and tensile strength of CFRP based on T-300 and XAS fibres (intermediate strength fibres) was noted [7, 9, 23, 24]. As a result it was supposed that the fibre compressive and tensile strengths are equal [9]. Similarly, from the fact that the strength of a composite reinforced by ultra-high strength T-800, T-1000 and IM-6 fibres is significantly lower than in tension [7, 24, 25], it is usually assumed that the compressive strength of these fibres is lower than their tensile strength.

2. Experimental procedure

As a reinforcement, different PAN-based high-strength carbon fibres (T-800, AS-4, UKN-5000A, UKN-5000B, UKN-5000C) and high-modulus M-40 and HM fibres were used. The tensile strength of UKN-5000 fibres increases in the sequence UKN-5000A < UKN-5000B < UKN-5000C (Table I). In order to investigate the effect of surface treatment, UKN-5000B fibres with different levels of surface treatment were used. As matrices, hot-setting EDT-10, EHD and EKT epoxy resins were used. EHD and EKT matrices have a higher rigidity and strength compared with conventional EDT-10 epoxy resin.

The compressive strength of CFRP was measured by two methods: (1) by compression of cylindrical rods of 9 mm diameter and turned central parts of 5 mm diameter ("dog-bone" specimens, Fig. 1a), and (2) by compression of end-tabbed samples with rectangular cross-section (2.5 mm × 10 mm, Fig. 1b). Dog-bone rods were loaded on butt-ends in the guides enabling distortion to be eliminated and splitting to be suppressed as far as possible. According to Puchkov *et al.* [10] this test allows the suppression of splitting of GFRP, to obtain strength values of the order of the composite shear modulus and to study GFRP behaviour at fibre buckling. The end-tabbed rectangular specimens were similar to ITTRI specimens. These samples will be termed "dog-bone" and "ITTRI" specimens, respectively.

TABLE I Mechanical characteristics of fibres

Fibre	Diameter	Modulus[a]	Strength[a]
UKN-5000A	8.0	235	2.40
UKN-5000B	8.0	235	3.20
UKN-5000C	8.0	245	4.20
T-800 (Torayca)	5.1	300	5.60
M-40 (Torayca)	6.0	400	3.80
HM	8.0	480	1.60

[a] In tension at 10 mm gauge length.

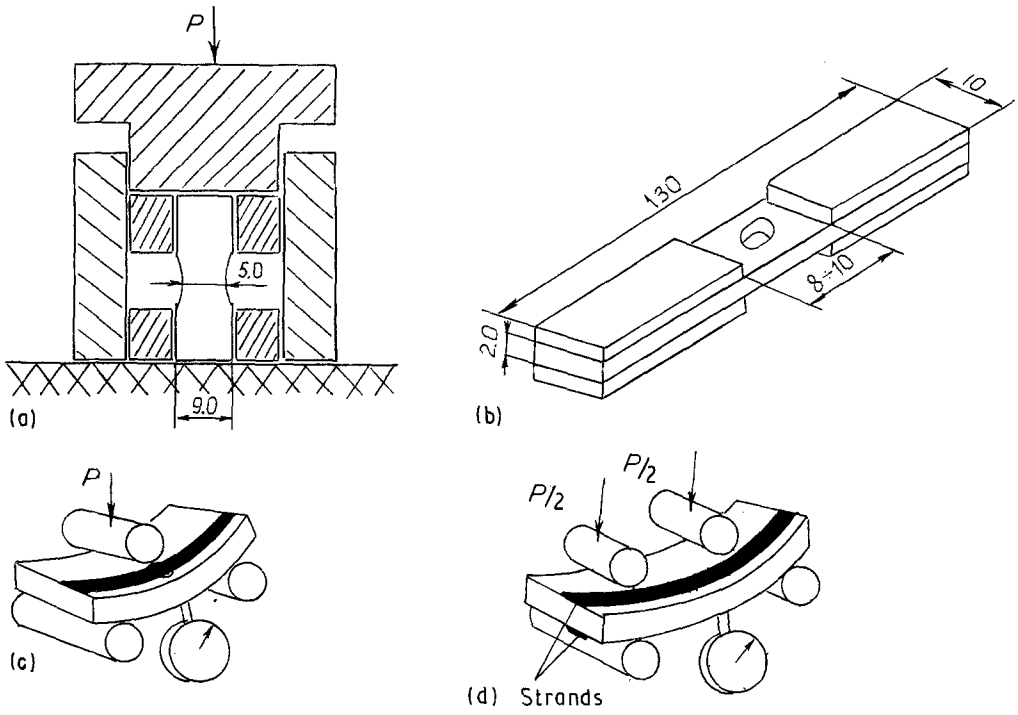

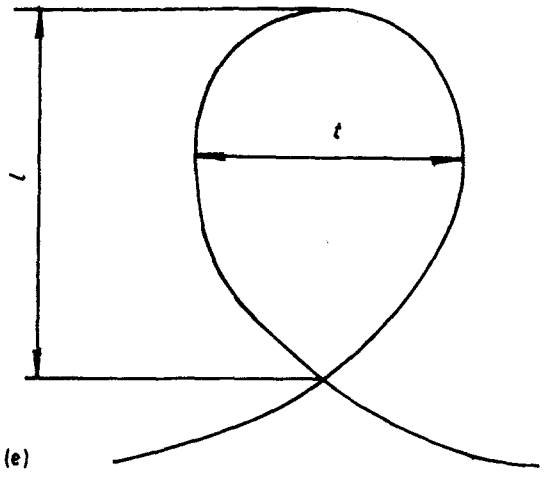

Figure 1 Test specimens. (a) "Dog-bone", (b) ITTRI, (c) three-point bending of a strand, (d) four-point bending of a strand glued to both tensioned and compressed surfaces of the beam, (e) the loop method, t and l are the loop transverse and longitudinal sizes.

Rectangular (ITTRI) specimens were made by winding filament preimpregnated with resin on a special rectangular mandrel with subsequent pressing up. The dog-bone specimens were obtained by pulling the matrix-impregnated thread of fibres into a cylindrical steel pipe of 9 mm i.d. After curing the matrix, the cylindrical rods were cut and subjected to turning. The fibre content was varied by controlling the fibre tension during winding of ITTRI specimens and by changing the amount of fibres pulled into the pipe in the case of dog-bone specimens. Each point was averaged after testing six samples.

Apart from these two test methods compressive strength was measured by bending an elastic glass fibre-reinforced plastic (GFRP) beam with a thin strand of carbon fibres glued to its compressed surface (Fig. 1c). The advantage of this method consists in the absence of any concentration of transverse and shear stresses in the strand, which may reduce the strength of the dog-bone and ITTRI samples [26, 27]. As a result, longitudinal splitting of the strands was suppressed. The beam was tested by three- and four-point bending. The GFRP beam width and thickness were 10 and 4 mm, respectively. In order to prevent the strand buckling, it was covered with a thin (0.1 mm) layer of epoxy resin. The strand thickness was about 20- to 25-fold lower than the beam thickness.

In three-point beam bending the critical radius of curvature of the strand was determined by: (1) measuring the deflection of the beam centre using the displacement pickup; (2) measuring the critical load at strand fracture moment; and (3) directly measuring the radius of curvature using the mould and templates.

In the first two cases the critical curvature radius, R^*, was determined according to [27]

$$R^* = L^2/12\,W \tag{2}$$

$$R^* = 3\,PL/E_c\,bh^3 \tag{3}$$

where W and L are the deflection and span of the beam corrected with regard for sliding from supports [27], P is the critical load, b and h are the width and thickness of the beam, E_c is the elastic modulus of the beam.

In order to investigate the relationship between the fibre compressive and tensile strengths directly, strands were glued upon both tensioned and compressed surfaces of the beam (Fig. 1d). This enabled us to measure simultaneously tensile and compressive strengths of the strand by the same method (four-point bending). The moment of strand fracture was determined with the help of a long focal length optical microscope ($\times$ 7). Strand fracture was followed by an acoustic "click".

For four-point bending the strand curvature was determined from the critical load, P

$$R^* = 6\,PA/E_b\,bh^3 \tag{4}$$

where A is the distance between the outer and inner rolls.

The fibre strength in the strand was calculated from

$$\sigma_f' = E_f \varepsilon^* = E_f h/2R^* \quad (5)$$

where E_f is the fibre elastic modulus.

Fibre compressive strength was additionally measured by the loop method in which both ends of the fibre were fixed precisely upon one axis. The loop was immersed into glycerin, and its longitudinal and transverse sizes (Fig. 1e) were measured by using an optical microscope. The maximum stress occurring at the loop tip is determined by radius of curvature of the fibre. In an elastic fibre the radius of curvature is proportional to the loop sizes [28]. This allows calculation of the fibre strength from the critical longitudinal size of the loop without direct determination of the radius of curvature. Using the theoretical results of Sinclair [28], the fibre strength may be found from

$$\sigma_f' = 1.43\, d_f\, E_f/l_c \quad (6)$$

where d_f is the fibre diameter, l_c is the longitudinal size of the loop at which the longitudinal/transverse size ratio, l/t, falls below 1.34. The fibre elastic modulus under compression was assumed to be equal to its tensile modulus. Results of the loop tests were averaged after examining five or six samples.

The composite shear strength was measured by three-point short-beam shear (ILLS) test at the span to thickness ratio = 5. To check the accuracy of the determined values, shear strength was also measured by torsion of unidirectional thin-walled tubes. A span to thickness ratio of 5 was chosen to provide close values of shear strengths determined by both methods. Fibre tensile strength was measured by testing a single fibre of 10 mm gauge length.

For temperature investigations, the dog-bone specimens were used. ITTRI specimens with circular holes were tested to investigate CFRP notch sensitivity. Shear modulus was measured using a torsion pendulum apparatus.

3. Results

3.1. Effects of fibre content and shear strength

Fig. 2 shows CFRP compressive strength plotted against carbon fibre volume content, V_f. The strength of composites reinforced by surface-treated fibres is directly proportional to the fibre content, V_f. In the case of untreated fibres, the strength asymptotically approaches its limiting value at high V_f. These results are completely in accordance with Hancox's data [4]. An increase in the fibre's tensile strength leads to a certain, although not very significant, increase in compressive strength of the dog-bone and ITTRI specimens. For example, the strength of a composite reinforced by super-strong T-800 fibres is only $\approx 10\%$ higher than in the case of UKN-5000B fibres. The strength difference of the dog-bone and ITTRI specimens may be neglected. Nevertheless, if the rectangular specimens without end tabs were used, the strength values were half these values. Thus the strength values are quite sensitive to the test method.

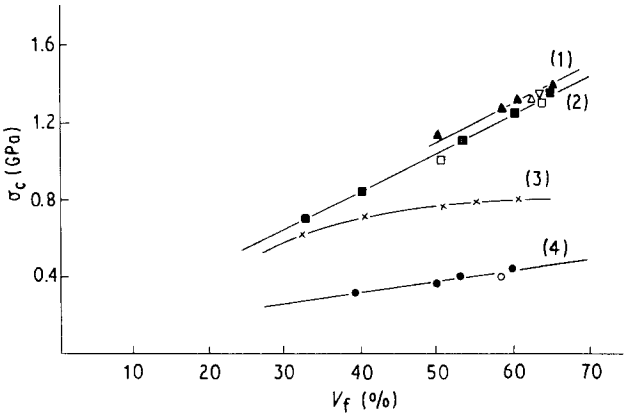

Figure 2 Compressive strength plotted against carbon fibre volume content, V_f. (1) (▲) T-800/EKT, dog-bone, (△) T-800/EKT, ITTRI, (▽) UKN-5000C/EKT, ITTRI. (2) (■) UKN-5000B/EKT, dog-bone, (□) UKN-5000B/EKT, ITTRI. (3) (×) UKN-5000B/EDT, surface untreated fibres. (4) (●) HM/EKT, dog-bone, (○) ITTRI.

However, sensitivity to the test method is typical for fracture modes controlled by the composite transverse and shear properties [10].

The strength of a composite reinforced by high-modulus fibres is much lower (Fig. 2). If one supposes that the composite strength is described by the mixture law (Equation 7), by extrapolation of the high modulus/EDT strength to $V_f = 100\%$, high-modulus fibre strength is estimated as $\sigma_f = 700$ MPa.

$$\sigma_c' = V_f \sigma_f' + V_m \sigma_m \quad (7)$$

where σ_m and V_m are the matrix strength and volume fraction.

Fig. 3 shows that the composite compressive strength, σ_c', is directly proportional to the shear strength, τ_c

$$\sigma_c' = A\, \tau_c \quad (8)$$

where $A = 14.5$.

Equation 8 is valid irrespective of the manner in which the shear strength was varied (using various

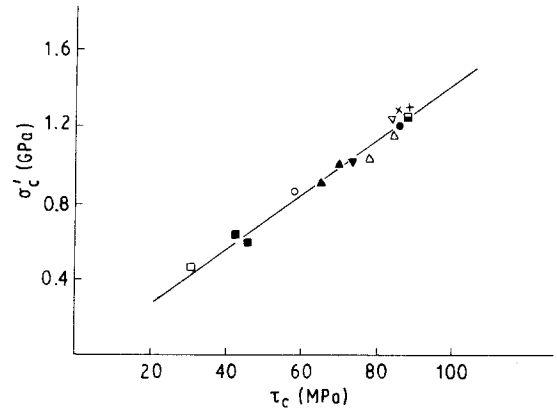

Figure 3 CFRP compression strength, σ_c' (dog-bone samples) plotted against shear strength, τ_c. (□) UKN-5000B/EKT, surface untreated fibres, ITTRI, (■) UKN-5000B/EDT, ITTRI, surface untreated fibres, (○) M-40/EKT, ITTRI, (▲) UKN-5000B/EDT, ITTRI, (▼) UKN-5000A/EDT, (△) UKN-5000B/EKT, ITTRI, (●) UKN-5000B/EHD, dog-bone specimens, (▽) UKN-5000C/EHD, dog-bone specimens, (×) T-800/EKT, ITTRI, (▣) UKN-5000C/EKT, dog-bone specimens, (+) T-800/EHD, dog-bone specimens.

matrices, fibres, different surface treatment, varying porosity, etc.). Compressive strength of CFRP based on high-strength EKT and EHD matrices is approximately 20% higher compared with the conventional EDT-10 matrix. Thus to obtain a high composite compressive strength, rigid matrices allowing high shear characteristics to be attained are needed.

3.2. Compressive strength of carbon fibres

3.2.1. Strand bending

Table II lists the results of different fibre strength measurements in strands. Fibre compressive strength depends neither on the strength determination method (via beam deflection, critical load or direct measurement of the curvature) nor on the test methods (three- or four-point bending). The mean compressive strength is equal to 3.9 ± 0.5 GPa for UKN-5000B, 4.6 ± 0.3 GPa for UKN-5000C, 5.8 ± 0.5 GPa for T-800 and 3.7 ± 0.4 GPa for M-40 fibres.

Two results are worth noting. First is the independence of strength on the matrix type (in the case of ITTRI and dog-bone specimens it is matrix sensitive). This may be explained by composite failure due to fracture of the fibres themselves. The second is the closeness of the strand compressive strength to its tensile strength (in the case of UKN-5000B and carbon fibres, compressive strength is even slightly higher). Compressive strength is close to tensile strength not only for intermediate strength (UKN-5000B) fibres but also for high-strength (UKN-5000C and T-800) and for high-modulus M-40 fibres. Further increase in fibre modulus (high-modulus fibres) leads to a reduction in compressive strength (0.8 ± 0.1 GPa) with respect to tensile strength (1.4 GPa). Fibre tensile strength was measured on 10 mm gauge length while compressive strength in a composite corresponds to an ineffective length [21] which is estimated to be ~ 2–4 mm. As a consequence, at beam bending the fibre strength corresponds to a shorter gauge length and this may be the reason why the compressive strength of UKN fibres is slightly higher than in tension.

To compare the fibre tensile and compressive strengths on the same gauge length, strands were tested by four-point bending with the strands glued both upon the compressed and tensioned surfaces of a beam (Fig. 1d). A simultaneous fracture of the strands on both surfaces of the beam was often registered. This occurred in 30% of the cases for T-800 strands and in 70% for UKN-5000C and M-40 fibres strands. In the remaining cases, random fracture of the strands was initially observed on the compressed or the tensioned surface of a beam. Thus, the fibre critical elongation at compression is equal to its elongation at tension (UKN-5000C, T-800, M-40). If the non-linear behaviour of a fibre at compression [29] is not taken into account, tensile and compressive strengths could be considered to be equal.

The results for high-modulus fibres ($E_f = 480$ GPa) are quite different. Compressive and tensile strengths of these fibres are not equal, the compressive strength being half the tensile strength. The compressive strength of high-modulus fibres in the strand is equal to 0.8 ± 0.1 GPa. This is in agreement with the value obtained in accordance with the mixture law (0.7 GPa). Hence the failure of ITTRI and dog-bone specimens is controlled by the high-modulus fibre strength.

3.2.2. Loop method

The non-linear behaviour of aramid fibres in a loop has been used to evaluate their compressive strength [30]. This method has been used by Jones and Johnson [29] to measure the tensile strength of high-strength carbon fibres at very short gauge length. Additionally, they found that the behaviour of high-modulus fibres in a loop is non-linear (linear for high-strength fibres). Non-linearity is connected with the

TABLE II Compressive strength of carbon fibres in a strand

Composite	Test method	Fibre compressive strength (GPa)				Tensile strength (GPa)
		Deflection	Critical load	Curvature	Mean	
UKN B/EKT	Three-point	3.5–3.8	3.5–3.8	3.6	3.6	–
UKN B/EDT	Three-point	4.0–4.4	4.4–4.5	–	4.3	–
UKN C/EDT	Three-point	4.5–4.8	4.5–4.8	4.6	4.7	–
UKN C/EKT	Three-point	4.4–4.5	4.4–4.5	4.5	4.5	–
UKN C/EHD	Three-point	4.5–5.0	4.5–5.0	–	4.9	–
UKN C/EDT	Four-point	–	4.4–5.0	4.3–4.6	4.6	4.5–4.9[a]
T-800/EDT	Three-point	5.3–5.8	5.3–5.8	5.8–6.4	5.7	–
T-800/EKT	Three-point	5.5–6.1	–	5.9	5.9	–
T-800/EHD	Three-point	6.0–6.5	5.8	–	6.0	–
T-800/EDT	Four-point	–	–	5.6–5.8	5.7	5.6–5.8[a]
M-40/EKT	Three-point	3.9	3.7–4.0	3.7	3.8	–
M-40/EDT	Three-point	3.3	–	–	3.3	–
M-40/EKT	Four-point	–	3.6–4.2	4.2–4.3	4.1	3.7–4.2[a]
HM/EDT	Three-point	0.70–0.85	–	–	0.8	1.3–1.5[b]

[a] In a glued strand.
[b] Strand was not glued.

steadily progressing growth of fracture disturbances from the fibre compressed side to its centre.

In the present paper, the loop test was used to measure compressive strengths of carbon fibres. For comparison, glass fibres which have absolutely elastic deformation were also tested (Fig. 4a). UKN-5000A fibres in a loop also produce an elastic deformation diagram up to failure. The results for UKN-5000B fibres are shown in Fig. 4b. It is difficult to conclude whether or not the behaviour of these fibres is elastic. At the same time the high-strength T-800 and high-modulus M-40 fibres exhibit a non-linearity, suggesting an inelastic character of deformation (Fig. 4c and d). Thus some carbon fibres have a non-linear behaviour in a loop and others do not. Non-linear behaviour is typical not only for high-modulus fibres, as was shown by Jones and Johnson [29], but also for new superhigh-strength T-800 fibres as well. The completely elastic deformation diagram of glass fibres proves that non-linearity is not a result of experimental error. Fibre compressive strength was calculated from Equation 6 to be 4.4 ± 0.6 GPa for T-800 and 3.5 ± 0.3 GPa for M-40 fibres. These values are considered to be the fibre compressive strengths (Table III). The strength of M-40 fibres is in agreement with that in strands, while T-800 fibre strength in loops (4.4 GPa) is lower than in strands (5.8 GPa). Unfortunately, we failed to apply the above method to high-modulus fibres ($E_f = 480$ GPa) owing to their extreme brittleness.

For the glass fibres the ratio t/l, where t and l are the loop transverse and longitudinal sizes, is precisely equal to 1.34 during tightening of a loop, while for the carbon fibres significant scatter in t/l is observed. This is presumably related to the slightly non-ideal cylindrical shape of a fibre and rigid "dirt" upon its surface which is detected using a scanning electron microscope (SEM).

3.3. The effect of circular holes

Fig. 5 shows CFRP compressive strength plotted against circular hole diameter, D. The relative strength decrease is described by the same curve at 40 and 60 vol % content. Fig. 6 shows that this dependence represents a straight line in double logarithmic coordinates. Hence strength is described by a power function

$$\sigma_c' = K/D^q \quad (9)$$

where K is a constant and $q = 0.38 \pm 0.04$ is the power index, which is close to 1/2. Consequently, the linear fracture mechanics describes the effect of stress concentrators on the CFRP compressive strength (it cannot be used for tension). This is quite unusual, as in traditional materials the former may be used for tension but not for compression. To describe the effect of defects for a multilayered CFRP, Guynn and Braydley [31] modified fracture mechanics using the point stress criterion developed by Waddoups *et al.* for

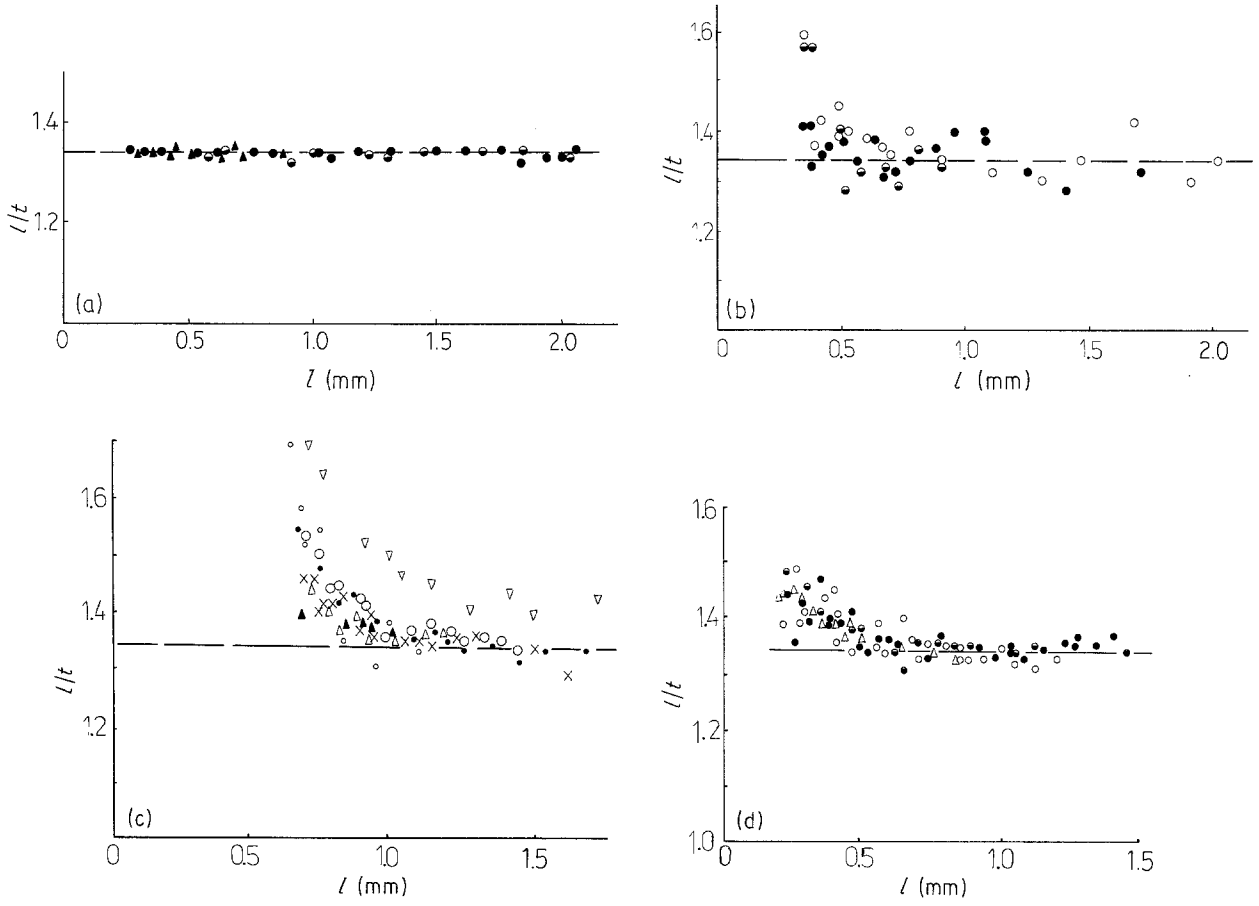

Figure 4 Ratio of loop longitudinal/transverse sizes, l/t, plotted against l for (a) glass, (b) UKN-5000B, (c) M-40 and (d) T-800 fibres. Different symbols represent different specimens.

TABLE III Fibre strength in a loop

Fibre	l_f (mm)[a]	l_c (mm)[b]	σ_f' (GPa)
T-800	0.22	0.45	4.4 ± 0.6
M-40	0.65	0.9	3.5 ± 0.3

[a] Fracture.
[b] Inelastic deformation.

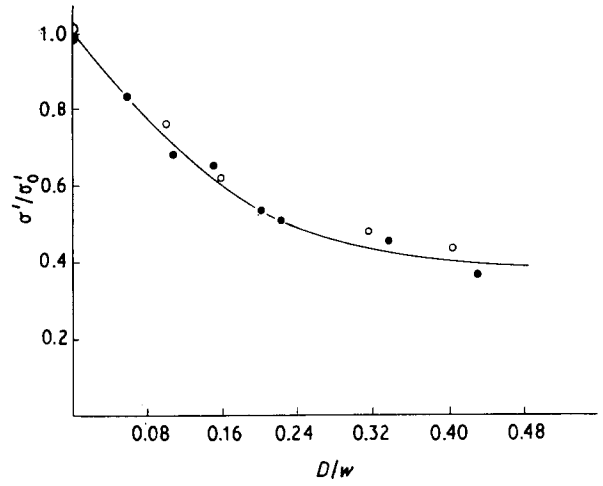

Figure 5 Compressive strength plotted against CFRP circular hole diameter; $w = 10$ mm is the sample width. (○) UKN-5000B/EKT, $\sigma_o' = 1.30$ GPa, $V_f = 60\%$, ITTRI. (●) UKN-5000B/EDT, $\sigma_o' = 0.75$ GPa, $V_f = 40\%$. ITTRI specimens.

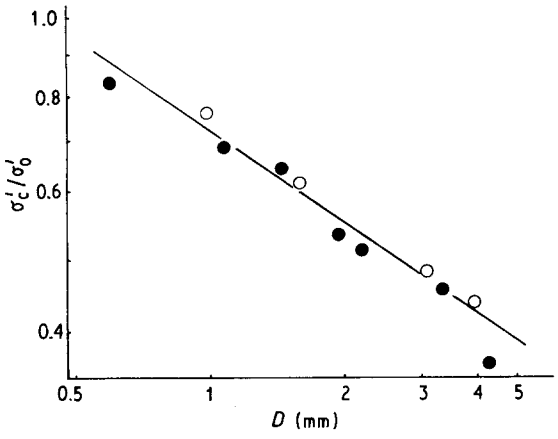

Figure 6 Compressive strength plotted against the hole diameter, D, in double logarithmic coordinates.

composites under tensile load [32]. For a unidirectional composite, modification of the linear fracture mechanics is not necessary.

The proportionality between the compressive and shear strengths, as well as the applicability of linear fracture mechanics to compression, may be explained if one assumes that a kink develops immediately after the emergence of the longitudinal crack. In samples with a hole at some critical compressive stress near the hole, four longitudinal splits appear (Fig. 7a). According to several reports [33–35], at tension the critical stress at which splits appear near a hole coincides with

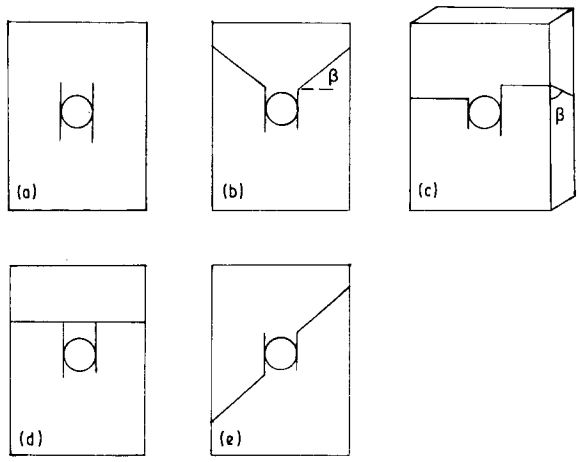

Figure 7 (a) Splitting near a circular hole, (b–e) typical appearance of fractured samples, β is the kink angle.

that for splitting near a crack. Splitting stress in both cases is described by linear fracture mechanics. In shear lag approximation, the critical stress at compression coincides with that for local splitting at tension. Hence compressive strength may be described by [35]

$$\sigma_c' = (E_c G_{IIc}/D)^{1/2} \quad (10)$$

where E_c is the composite elasticity modulus, G_{IIc} is mode II fracture toughness and D is the diameter of the hole.

Observation of the fracture process revealed that the emergence of splits near a hole does lead to kinking. Typical appearances of fractured samples are shown in Fig. 7b–e. Sometimes emergence of kinks was observed in the vicinity of the hole, while no visible splitting was observed. We suppose that in this case the split was so short that it was not detected. A kink originating by a very short split was observed by Rhodes *et al.* [36].

3.4. Effect of temperature

Fig. 8 shows the variation of compression strength with temperature. Near the matrix glass transition temperature, T_g, strength sharply decreases due to matrix softening, which is illustrated by the temperature dependence of composite shear modulus (curve 2). The dependencies of compressive strength and shear modulus are similar.

At $T > T_g$ the dependence of strength on fibre content, V_f, is not linear. Fig. 9 shows that this dependence becomes linear in coordinates $\sigma_c' - (1 - V_f)^{-1}$. Consequently, the strength is proportional to the composite shear modulus in accordance with Equation 1. The coefficient of proportionality for the straight line in Fig. 9 is equal to 104 MPa. This value is quite close to the matrix shear modulus $G_m \approx 120$ MPa. By extrapolation of the straight line to $V_f = 0$ one obtains $\sigma_c = 120 \pm 15$ MPa. This value is also close to G_m. Thus Equation 1 quite accurately describes CFRP compressive strength on V_f at $T > T_g$. Hence one can

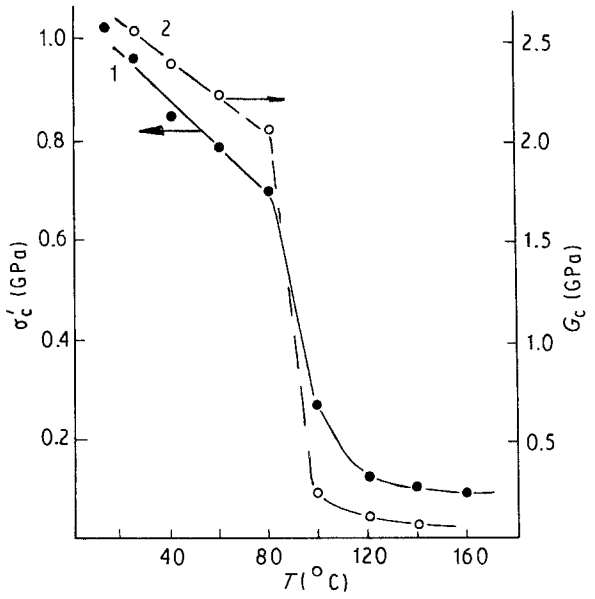

Figure 8 UKN-5000B/EDT: (1) compressive strength, σ_c', and (2) modulus of elasticity at torsion, G_c plotted against temperature; (1) strength, $V_f = 46$ vol %; (2) torsion modulus, $V_f = 35$ vol %.

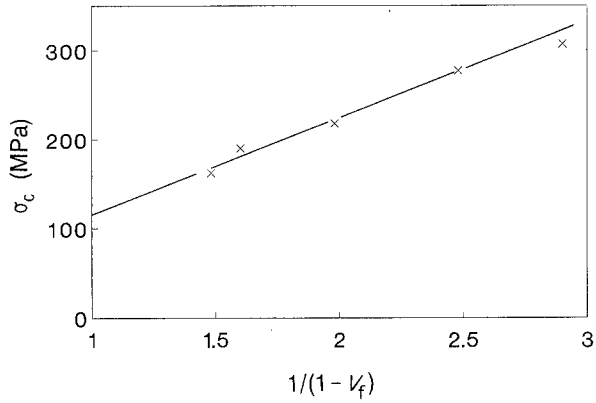

Figure 9 Compressive strength at $T = 110\,°C$ plotted against $(1 - V_f)^{-1}$. EDT-10 matrix, $T_g = 90\,°C$ (see Fig. 8).

conclude that the failure mode at elevated temperatures is fibre buckling.

3.5. Fracture

At room temperature, irrespective of the type of fibre and matrix, failure is a result of the appearance of a kink band (Figs 10, 11a and b). The fracture of the dog-bone specimens often follows splitting of specimen's cylindrical working part (Fig. 12). Single or multiple kinks appear in the vicinity of the compressing surface (sample facet). ITTRI samples often fracture in the vicinity of end tabs.

In rectangular ITTRI samples the kink can propagate both in front and side planes (Fig. 7b and c). It was found that the kink propagation angle β is equal for "front" and "side" planes. Within an accuracy of ± 4°, β (= 39 ± 4° for dog-bone specimens) does not depend on the type and strength of fibres (UKN-5000A, B, C, T-800, M-40, HM) and matrix (EDT, EKT, EHD). Values of β were the same for samples with and without stress concentrators. In the case of the dog-bone specimens, β = 33 ± 4° which is somewhat lower than the value obtained for ITTRI specimens. The reason why β depends on the test method is not clear. Hahn [37] predicted the dependence of the kink length and β on the fibre type. The kink length, L_c (Fig. 10), significantly varies (from 30–60 μm), and no dependence of L_c on the fibre and matrix properties at room temperature was noticed. However, an increase in temperature was followed by two-fold growth in fractured piece lengths at $T > T_g$. This indicates that the kink length does depend on matrix properties but the dependence is very weak. The kink length and angle β (≈ 35°) in a strand was close to these in ITTRI samples. Fig. 11d shows that the fibre fracture in the kink tip is followed by fibre bend fracture.

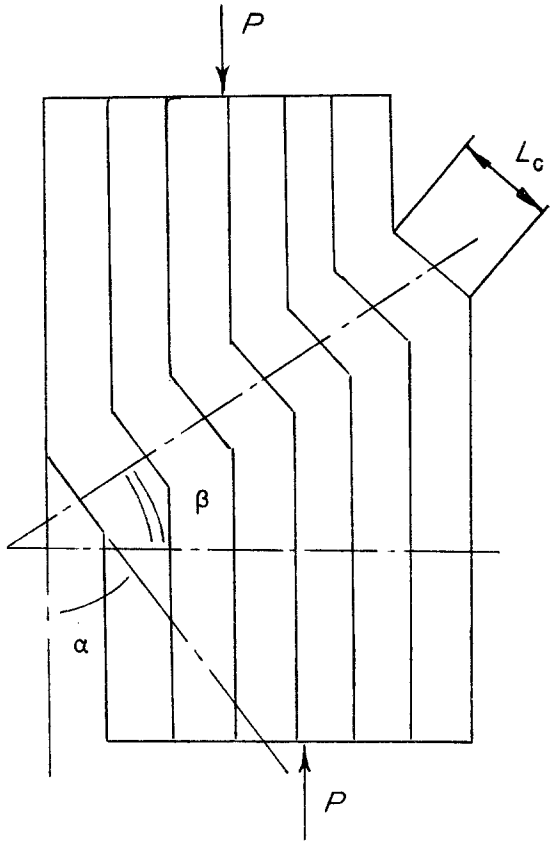

Figure 10 Kink, L_c = kink length, $\alpha = 2\beta$.

Each kink band consists of one or several parallel step-like "elementary kinks" of fixed length (30–60 μm). Broken fibre parts in the neighbour elementary kinks in the same band are parallel (Fig. 11c).

According to Wolla and Goree [34], fractographic analysis of the fracture surface of individual fibres in a kink allows one to conclude whether the final step of a failure is a result of tension, compression or bending of the fibres. If parallel fracture lines are detected upon the facets of single fibres in a kink, it can be concluded [38] that finally a fracture of all types of fibre in a kink is caused by their bending. Sometimes two adjacent kinks which propagated not parallel but in different directions were also observed.

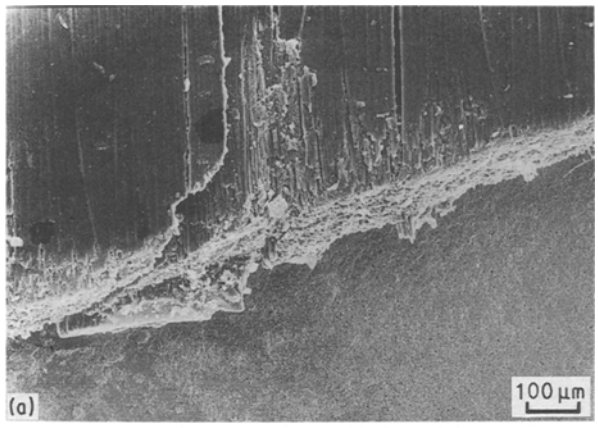

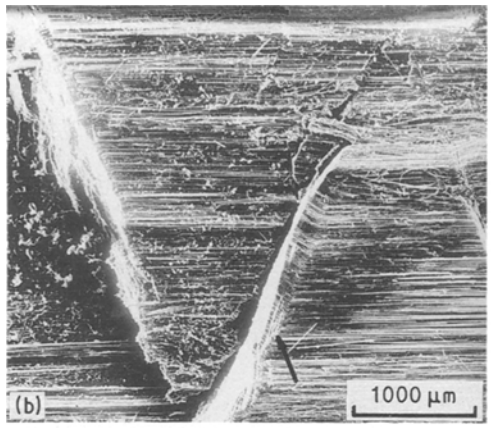

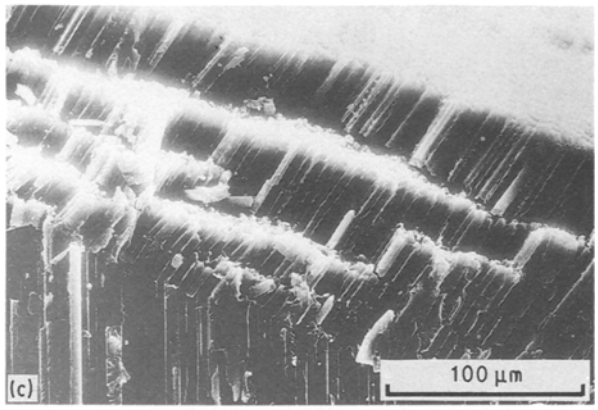

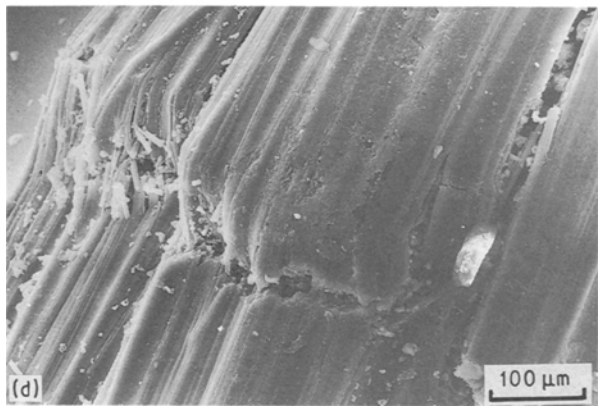

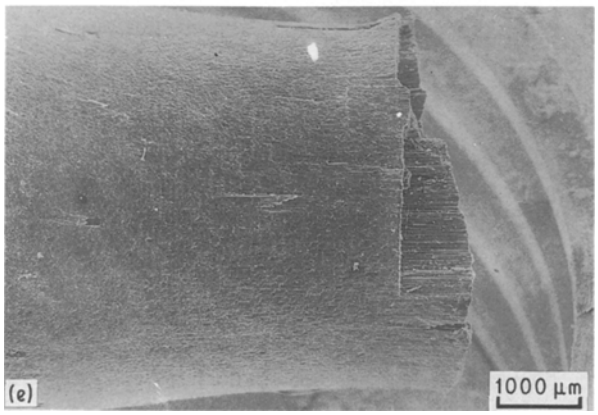

Figure 11 (a, b) Fractured dog-bone specimens, (c) kinks steps ("elementary kinks"), magnified area shown by the arrow in (b), (d) kink tip in a strand, (e) sample fractured at $T = 110\,°C$.

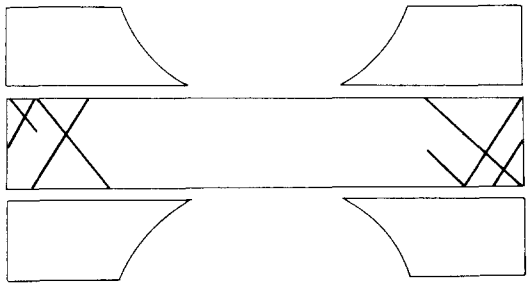

Figure 12 Schematic fracture of dog-bone specimens.

The fracture of a composite reinforced by high-modulus fibres has two peculiarities. The first is the fracture in a working part, both in dog-bone and ITTRI specimens, and the absence of any longitudinal splitting. The second is the equality of fibre strength in strands and rods. This indicates that in this case kinking is stimulated not by splitting but by high-modulus fibre bearing-capacity loss.

3.6. Fracture at elevated temperature

Near the matrix T_g the fracture mode changes, together with the angle, β, between the fibre axis and the fracture band. The angle β at $T > T_g$ is close to 0° (Figs 11e and 13) and the fracture band propagates practically perpendicular to the fibre axis. This band is a result of a wave of local fibre buckling. The length of broken fibres in this band is about 80–100 µm, which

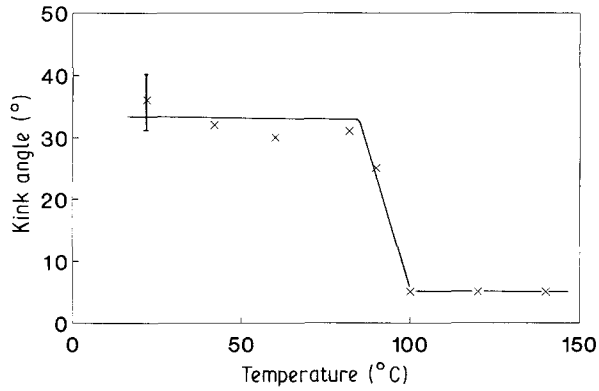

Figure 13 Angle between the kink planes in rectangular cross-section specimens plotted against temperature, T.

is approximately the double kink length at room temperature. At room temperature, fibre bend with respect to the kink plane is antisymmetrical (Figs 10 and 11c) while above T_g the fibre bend in it is symmetrical (Fig. 11e). For this reason, Bazhenov *et al.* [22] termed the fracture band at $T > T_g$ a "symmetrical kink". Note that β is close to 0° but is not exactly equal to 0. The fracture band at $T > T_g$ resembles a spiral shape with $\beta = 5°–8°$.

4. Discussion

Nearly a two-fold increase in the tensile strength of fibres results in a minor ($\sim 10\%$) increase in the rods compressive strength (UKN-5000A/EDT – T-800/EDT). The present data suggest that in this sequence the composite compressive strength is limited not by the fibres properties but is a consequence of the emergence of the first longitudinal split along the loading direction. The stress at which splitting starts is determined by shear strength. As a result, compressive strength is proportional to shear strength. In samples with a hole, strength is determined by stress at which longitudinal splits appear near the hole. Fracture is a consequence of the appearance of these splits and the strength is described by linear fracture mechanics.

Kink initiation by longitudinal splitting may be explained by fibre bending in the tip of the split (Fig. 14a) and by propagation of the split not exactly along the fibres but across some of them. If several neighbour fibres in the crack tip are fractured, an unstable growth of the kink may start due to concentration of bending stress and the "domino" effect when the fracture of one fibre provokes the fracture of its neighbours.

Fibre bending in the tip of a crack oriented transversely to the fibre direction under tension was investigated theoretically by Kobelev [39]. Theoretical equations of elasticity are reversible to load sign change and Kobelev's results [39] may also be applied to compression. In the case of splitting under compression, the cause of fibre bending is presumably quite different. Near a hole the longitudinal compressive stress is zero on one side of the split and equal to external compressive stress on the opposite side. As a result, growth of the split near a hole is accompanied by shear of the crack on opposite sides. As the split surface is quite rough, cracking leads to transverse displacement of the split sides and to bending of bridging fibres in its tip (Fig. 14a). Of course in the case of samples without a stress concentrator, shear of the opposite sides of the split is not so high. Nevertheless, in this case, external stress is much higher and even slight fibre bending in the split tip stimulates fibre fracture.

The compressive strengths of UKN and M-40 fibres are equal to their tensile strengths. This confirms the Reinolds and Sharp model [40], according to which carbon fibre failure is initiated by shear in misoriented graphite crystallites. On the contrary, high-modulus fibre results contradict this model.

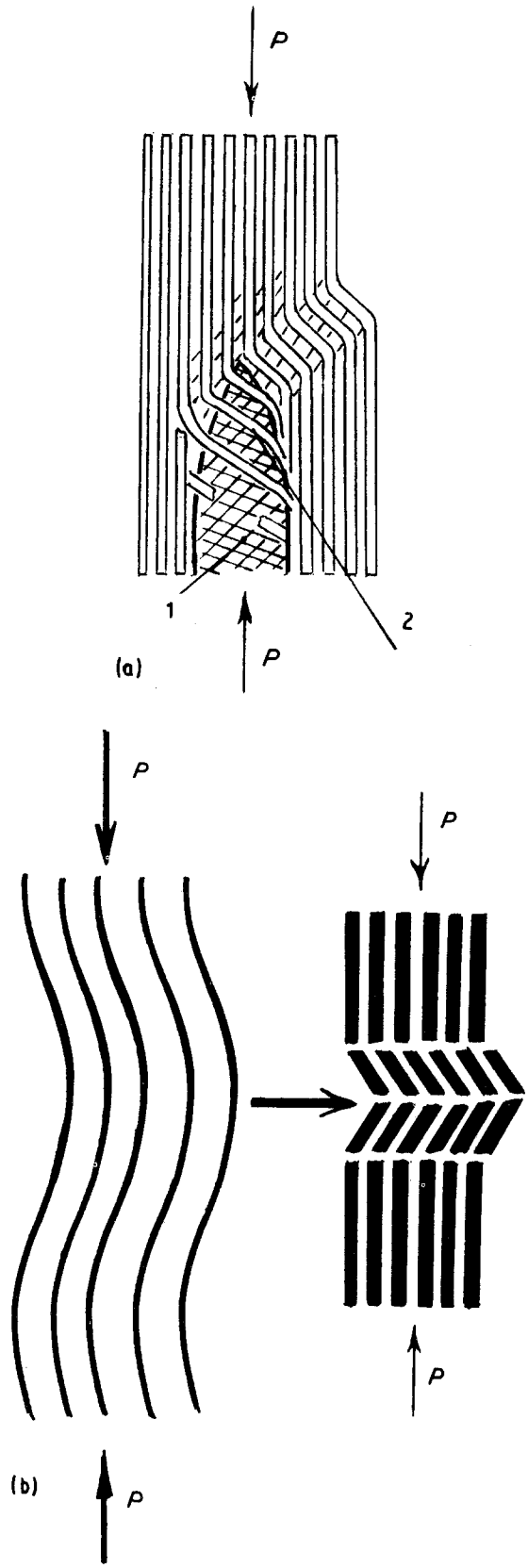

Figure 14 Kinking model. (a) Initiation of a kink near the tip of a longitudinal split: (1) split, (2) bent fibres in the split tip. (b) Initiation of a "symmetrical kink" by fibre buckling at $T > T_g$.

The difference in T-800 fibre strength values measured by the loop method and by beam bending should be noted. This difference may result from non-Hookean behaviour of the fibres in compression [29] due to which in bending the strength may be overestimated (Equation 5). Consequently, strand bend

gives an upper limit of the fibre strength. On the contrary, the recoil method and the method used by Oshama *et al.* [20] give underestimated values. More reliable methods seem to be the testing of a fibre embedded in matrix and the loop test. Of course these methods also have essential disadvantages and are not precise. The strength of an embedded fibre may be overestimated due to the matrix support effect [22]. In loops, strength may also be overestimated due to non-uniform distribution of stress over the fibre cross-section and a decrease in compressive stresses to the fibre centre. For example, in the case of aramid fibres, these methods give 1.5–2-fold overestimation of fibre strength. Of course, in the case of carbon fibres due to their much higher fibre strength, the error is supposed to be less. Additionally these tests may also give underestimated strength values. According to Hawthorne and Teghtsoonian [16] fibre fracture begins with the appearance of round cracks on the surface of the fibre. Further loading of an embedded fibre produced a gradual coarsening of the cracks until eventually they developed into a distinct shear of the fibre ends past each other. Hence, it is not clear at which moment the fibre load-bearing capacity is lost, and if the fibre strength is calculated from the strain at which first fracture event starts, the strength may be partly underestimated. We suppose that for carbon fibres errors leading to strength overestimation, on the one hand, and to its underestimation, on the other, may partly compensate each other. Nevertheless, precise and reliable measurement of fibre compressive strength still remains a problem.

The strand strength does not depend on the matrix properties. Consequently, it does not correlate with shear strength and failure is caused not by splitting but by a compressive fracture of the fibres.

Fig. 15 shows the correlation between fibre tensile and compressive strengths. For high-modulus fibres, compressive strength is lower than tensile strength. The strengths of intermediate and high-strength fibres (UKN-5000A, B and C, M-40) are close. In super-strong T-800 fibres, some decrease in compressive strength compared with tensile strength might be noted.

Fig. 16 shows the dependence of CFRP compressive strength on fibre strength. In the case of low-strength high-modulus and UKN-5000A fibres, composite strength is described by the mixture law $\sigma'_c = V_f \sigma'_f$ (Equation 7). With an increase in fibre strength, the composite strength remains practically constant due to composite splitting. In this case composite strength is determined by matrix properties and the fibre strength does not affect composite properties. As a result, composite strength values are essentially lower than those predicted by the mixture law. Note that the strength of high-modulus M-40 fibre-reinforced composite is not described by the dependence applicable for other composites. This is explained by the lower adhesion of high-modulus fibres to the epoxy matrix and the lower shear properties of the composite. Thus, at some fibre strength (Fig. 16) the composite failure mode is changed. The fibre strength

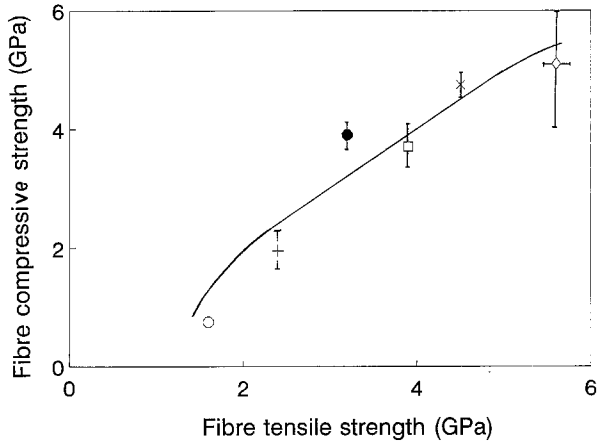

Figure 15 Correlation between fibre tensile and compressive strength. (○) High-modulus fibre, (+) UKN-5000A, (●) UKN-5000B, (□) M40, (×) UKN-5000C, (◇) T-800.

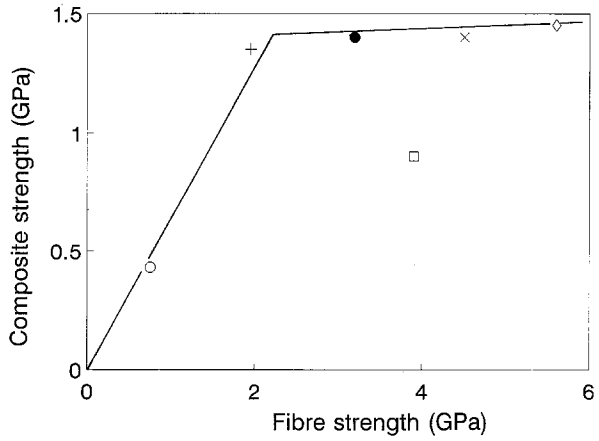

Figure 16 Dependence of CFRP compressive strength on fibre compressive strength. (○) High-modulus fibre, (+) UKN-5000A, (●) UKN-5000B, (□) M40, (×) UKN-5000C, (◇) T-800.

at which the fracture mode changes may be roughly evaluated from the mixture law. A typical value of CFRP compressive strength is equal to 1.4–1.8 GPa at ~ 60 vol % fibre content [7]. Consequently, the fracture mode changes at fibre strength approximately equal 2.5–3 GPa. At low fibre strength, the composite failure mode may be termed "fibre fracture-induced kinking" and at high fibre strength "split-induced kinking".

In both cases, kinking is not connected with fibre buckling, which takes place only at elevated temperature when the matrix elasticity is very low (Equation 1). There are three cases when failure mode is definitely fibre buckling. The first is failure of dog-bone specimens of glass fibre-reinforced plastic when sample splitting is suppressed [10]. The crack in this case propagates perpendicular to the fibres. The second case is failure of organic fibre-reinforced plastic at $T > T_g$. The fracture band in this case also propagates practically perpendicular to the fibres [22]. The third case, fracture of CFRP at $T > T_g$, is analogous to that of aramid fibre-reinforced plastic and $\beta \approx 0°$. Thus propagation of the fracture band perpendicular to fibres and appearance of "symmetrical kink" (Figs

11e and 14b) was observed in all three cases when the cause of failure was fibre buckling.

According to Bazhenov *et al.* [22], at room temperature, kinking of aramid FRP is caused by fibre yield fracture. In CFRP, kinking is caused either by fibre fracture or by composite splitting. Both in OFRP and CFRP kinking was never connected with fibre buckling. We suppose that this is not a coincidence. This supposition is confirmed by analysis of the theoretical results of Budiansky [41]. He considered a cooperative fibre buckling wave at an angle, β, to the load direction [41] and obtained the following equation for the critical stress

$$\sigma_c' = G_c + E_t \tan^2\beta \quad (11)$$

where G_c is the elastic shear modulus of the composite, and E_t is transverse modulus.

Strength is minimum at $\beta = 0°$. Consequently, at fibre buckling, a fracture band propagates perpendicular to the load direction. The second conclusion is that kinking is not connected with fibre buckling and, consequently, it is connected with some other causes.

The transition from "splitting" to "kinking" of CFRP was discussed earlier [8, 9]. It has been shown that an external pressure suppresses "splitting", leading to a significant increase in strength, and to "kinking". Of course "splitting" and "kinking" are essentially different fracture mechanisms. Nevertheless, the difference between these two fracture modes in the case of high-strength fibres is less fundamental than between "kinking" stimulated by a split and "kinking" stimulated by a fibre fracture. "Splitting" is probably a fracture mode when the first longitudinal split does not lead to kinking because the concentration of bend stresses in the split tip is not sufficiently high. "Splitting" is possible only in test methods which do not allow achievement of high strength values. Thus in the case of high-strength fibres, "kinking" and "splitting" are but two different stages of "splitting".

Fig. 17 shows that CFRP compressive strength plotted against the square root of porosity (the data were taken from Hancox [4]) gives a straight line

$$\sigma_c'/\sigma_o' = 1 - BV_p^{1/2} \quad (12)$$

where $B = 1.5$ is an experimental constant, V_p is the pore volume content and σ_o is the strength at $V_p = 0$.

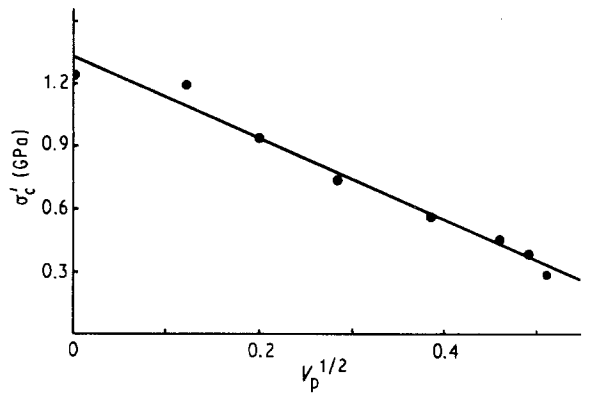

Figure 17 Compressive strength, σ_c', plotted against square root of fibre content, $V_p^{1/2}$. Data are taken from Hancox [4].

This dependence coincides with that for GFRP at "splitting" fracture mode [10]. Owing to the non-linear dependence of σ_c' on V_p, pores lead to very sharp reduction in compressive strength. For example, 1 and 4 vol % pores result in 15% and 30% strength decrease.

One effect of pores on CFRP shear strength is described by the same square root function [42]

$$\tau_p/\tau_o = 1 - BV_p^{1/2} \quad (13)$$

where $B = 1.65$ and τ_o is the shear strength at $V_p = 0$. B coefficients values for compressive and shear strengths are very close (1.5 and 1.65). Thus the effect of pores on the compressive and shear strengths is the same. As a result, the direct proportionality between σ_c' and τ_p (Equation 7) remains valid. Equation 13 may be explained if one supposes that pores are cylindrical in shape, have regular square arrangement and that the crack grows through the plane in which pore cross-section is maximum, i.e. through the pore centre. The pore's part in this plane is equal to $\alpha = (4V_p/\pi)^{1/2}$ [42]. As the strength is proportional to the material cross-section (minus pore area) in the fracture plane, the following equation may be written

$$\tau_c/\tau_o = 1 - \alpha = 1 - (4/\pi)^{1/2} V_p^{1/2} \quad (14)$$

Equation 14 agrees with experiment if $B = (4/V_p)^{1/2} \sim 1.2$. The experimental value of B (1.65) is quite close to the theoretical one (1.2).

Thus there are four different failure modes of fibre-reinforced plastics under compression: (1) fibre buckling; (2) longitudinal splitting, (3) kinking due to fibre fracture, and (4) kinking due to composite splitting. Table IV summarizes the conditions under which different modes of composite failure are realized, and describes the main features of these fracture modes.

5. Conclusions

1. New failure mode of CFRP has been found. In composites reinforced with high-strength fibres or in the presence of stress concentrators, a kink is initiated by longitudinal splitting.

TABLE IV Fracture modes of CFRP in compression

	Kinking stimulated by		Fibre buckling[c]
	Splitting[a]	Fibre fracture[b]	
High temperature	–	–	+
Stress concentrator	+	–	–
Low-strength fibres	–	+	–
High-strength fibres	+	–	–

[a] Kink at 30°–40° to the load axis; strength is proportional to shear strength; strength is lower in comparison with composite tensile strength.
[b] Kink at 25°–40° to load axis; compressive and tensile strengths are equal.
[c] "Symmetrical kink" perpendicular to fibre axis; strength is close to composite shear modulus.

2. In the case of low-strength fibres, kinking is a post-effect whereas the true failure cause is the compressive fracture of the fibres.

3. The effect of stress concentrators upon unidirectional carbon fibre-reinforced plastic under compressive load may be described by the Griffith's criterion.

4. At elevated temperatures the failure is a result of fibre buckling. The most characteristic feature of this fracture mode is the appearance of a fracture band ("symmetrical kink") perpendicular to the direction of fibre orientation.

5. The strand bending test gives a fibre-controlled upper limit of the composite compressive strength. The loop method may also be used to measure the compressive strength of the carbon fibre.

References

1. N. F. DOW and T. S. GRUNTFEST, "Determination of Most Needed Potentially Possible Improvements in Materials for Ballistic and Space Vehicles", General Electric Co., Space Science Laboratory, TJS R 60 SD 389 (1960).
2. A. L. RABINOVICH, in "Proceedings of MPTI", edited by V. Petzov (Oborongiz, Moscow, 1961) N7, p. 3.
3. M. R. PIGGOTT, in "Developments in Reinforced Plastics", Vol. 4, edited by G. Pritchard (Elsevier Applied Science, London, New York, 1984) p. 131.
4. N. L. HANCOX, *J. Mater. Sci.* **10** (1975) 234.
5. S. KUMAR, W. W. ADAMS and T. E. HELMINIAK, *J. Reinf. Plast. Compos.* **7** (1988) 108.
6. I. PETKER, *SAMPE Q.* **3** (1972) 7.
7. R. DIEFENDORF, in "Carbon Fibres and Their Composites", edited by E. Fitzer (Springer-Verlag, Berlin, Tokyo, 1985) p. 62.
8. C. W. WEAVER and J. G. WILLIAMS, *J. Mater. Sci.* **10** (1975) 1323.
9. T. V. PARRY and A. S. WRONSKI, *ibid.* **17** (1982) 893.
10. L. V. PUCHKOV, S. L. BAZHENOV, A. M. KUPERMAN, A. A. BERLIN and E. S. ZELENSKII, *Dokl. Akad. Nauk SSSR* **284** (1985) 349.
11. P. D. EVINS, Royal Aircraft Establishment Technical Report. no. 70007 (1970).
12. E. M. de FERRAN and B. HARRIS, *J. Compos. Mater.* **4** (1970) 62.
13. R. L. SIERAKOWSKI, G. E. NEWILL, C. A. ROSS and E. R. JONES, *ibid.* **5** (1971) 362.
14. L. B. GRESZCZHUK, in "Strength and Fracture of Composites", Proceedings of the 2nd Soviet-American Symposium on Composites, March 1981, Bethlehem, Pennsylvania, edited by G. C. Sih and V. P. Tamuzh (Zinatne, Riga, 1983) p. 304 (in Russian). [American version, edited by G. C. Sih (Martinus Nijhoff, The Hague, 1981) p. 231.]
15. A. S. ARGON, in "Treatise on Materials Science and Technology", Vol. 1, edited by H. Liebowitz (Academic Press, New York, London, 1972) p. 106.
16. H. HAWTHORNE and E. TEGHTSOONIAN, *J. Mater. Sci.* **10** (1975) 41.
17. H. T. HAHN and M. M. SOHI, *Compos. Sci. Technol.* **27** (1986) 25.
18. S. R. ALLEN, *J. Mater. Sci.* **22** (1987) 853.
19. S. KUMAR, W. W. ADAMS and T. E. HELMINIAK, *J. Reinf. Plast. Compos.* **7** (1988) 108.
20. T. OSHAWA, M. MIWA, M. KAWADE and E. TSUSHIMA, *J. Appl. Polym. Sci.* **39** (1990) 1733.
21. A. KELLY and W. R. TISON, *J. Mech. Phys. Solids* **14** (1966) 177.
22. S. L. BAZHENOV, V. V. KOZEY and A. A. BERLIN, *J. Mater. Sci.* **24** (1989) 4509.
23. R. K. KLARK and W. B. LISAGOR, ASTM STP 734 (American Society for Testing and Materials, Philadelphia, PA, 1981) p. 34.
24. T. HIRAMATSU, T. HIGUCHI and J. MATSUI, in "Looking Ahead for Materials and Processes" (Elsevier, Amsterdam, 1987) p. 1.
25. J. MATSUI, S. NAMURA and Y. ISHII, *J. Jpn. Soc. Compos. Mater.* **12** (1986) 11.
26. D. H. WOOLSTENCROFT, A. R. CURTIS and R. I. HARESCENGH, *Composites* **12** (1981) 275.
27. J. M. TARNOPOLSKII and T. J. KINZIS, "Methods of Reinforced Plastics Testing" (Nauka, Moscow, 1981) p. 263 (in Russ.).
28. D. SINCLAIR, *J. Appl. Phys.* **21** (1950) 380.
29. W. R. JONES and J. W. JOHNSON, *Carbon* **9** (1971) 645.
30. J. H. GREENWOOD and P. G. ROSE, *J. Mater. Sci.* **9** (1974) 1809.
31. E. G. GUYNN and W. L. BRAYDLEY, *J. Compos. Mater.* **23** (1989) 479.
32. M. E. WADDOUPS, J. R. EISENMANN and B. E. KAMINSKI, *ibid.* **5** (1971) 446.
33. J. W. MAR and K J. LIN, *ibid.* **13** (1979) 278.
34. J. M. WOLLA and J. G. GOREE, *ibid.* **21** (1987) 49.
35. A. A. BERLIN, V. A. TOPOLKARAEV and S. L. BAZHENOV, in "Physical Aspects of Fracture and Deformation of Composite Materials", edited by A. M. Leksovsky (FTI, Leningrad, 1987) p. 102.
36. M. D. RHODES, M. M. MIKULAS and P. E. McGOWAN, *AIAA J.* **22** (1984) 1283.
37. H. T. HAHN, in Proceedings of the 6th International Conference on Composite Materials", Vol. 1, edited by F. L. Matthews, N. C. R. Buskell, J. M. Hodgkinson and J. Morton, London, July 1987 (Elsevier Applied Science, London, New York, 1987) p. 269.
38. L. SHIKHMONTER, I. ELDROR and B. CINA, *J. Mater. Sci.* **24** (1989) 167.
39. V. V. KOBELEV, *Mech. Compos. Mater.* (1988) 232.
40. W. N. REINOLDS and J. V. SHARP, *Carbon* **12** (1974) 103.
41. B. BUDIANSKY, *Comput. Struct.* **16** (1983) 3.
42. S. L. BAZHENOV and V. V. KOZEY, *J. Mater. Sci.* **26** (1991).

Received 25 July
and accepted 27 July 1990